



1 A comprehensive assessment of electrochemical ocean alkalinity
2 enhancement in seawater: kinetics, efficiency, and precipitation
3 thresholds
4

5 Mallory C. Ringham¹, Nathan Hirtle¹, Cody Shaw¹, Xi Lu¹, Julian Herndon^{2,3}, Brendan R. Carter^{2,3},
6 Matthew D. Eisaman^{4,5}
7

8 ¹ Stony Brook University, Stony Brook, NY, USA

9 ² Cooperative Institute for Climate Ocean and Ecosystem Studies, University of Washington, Seattle, USA

10 ³ Pacific Marine Environmental Laboratory, National Oceanic and Atmospheric Administration, Seattle, WA, USA*

11 ⁴ Department of Earth & Planetary Sciences, Yale University, New Haven, CT, USA

12 ⁵ Yale Center for Natural Carbon Capture, Yale University, New Haven, CT, USA

13 * Coauthors with this affiliation are included provisionally pending institutional manuscript policy review
14

15 *Correspondence to:* Mallory Ringham (mallory.ringham@stonybrook.edu); Current address: Ebb Carbon Inc., San
16 Carlos, CA, USA

17 **Abstract**

18 Ocean alkalinity enhancement (OAE) is a promising approach to marine carbon dioxide removal (mCDR) that
19 leverages the large surface area and carbon storage capacity of the oceans to sequester atmospheric CO₂ as dissolved
20 bicarbonate (HCO₃⁻). The SEA MATE (Safe Elevation of Alkalinity for the Mitigation of Acidification Through
21 Electrochemistry) process uses electrochemistry to convert some of the salt (NaCl) in seawater or brine into aqueous
22 acid (HCl), which is removed from the system, and base (NaOH), which is returned to the ocean with the remaining
23 seawater. The resulting increase in seawater pH and alkalinity causes a shift in dissolved inorganic carbon (DIC)
24 speciation toward carbonate and a decrease in the surface-ocean pCO₂. The shift in the pCO₂ results in enhanced
25 CO₂ uptake or reduced CO₂ loss by the seawater due to gas exchange. The net result of this process is the increase of
26 surface-ocean DIC, where it is durably stored as mostly bicarbonate and some carbonate. In this study, we
27 systematically test the efficiency of CO₂ uptake in seawater treated with NaOH at beaker (1L), aquaria (15L), and
28 tank (6000L) scales to establish operational boundaries for safety and efficiency in scaling up to field experiments.
29 Preliminary results show CO₂ equilibration occurred on order of weeks to months, depending on circulation, air
30 forcing, and air bubbling conditions within the test tanks. An increase of ~0.7-0.9 mol DIC/ mol added alkalinity (in
31 the form of NaOH) was observed through analysis of seawater bottle samples and pH sensor data, consistent with
32 the value expected given the values of the carbonate system equilibrium calculations for the range of salinities and
33 temperatures tested. Mineral precipitation occurred when the bulk seawater pH exceeded 10.0 and Ω_{aragonite} exceeded
34 30.0. This precipitation was dominated by Mg(OH)₂ over hours to 1 day before shifting to CaCO_{3, aragonite}
35 precipitation. These data, combined with models of the dilution and advection of alkaline plumes, will allow for
36 estimation of the amount of carbon dioxide removal expected from OAE pilot studies. Future experiments should
37 better approximate field conditions including sediment interactions, biological activity, ocean circulation, air-sea gas
38 exchange rates, and mixing-zone dynamics.

39 **Keywords**

40 Ocean Alkalinity Enhancement (OAE); marine carbon dioxide removal (mCDR); ocean carbon dioxide removal
41 (ocean CDR)

42



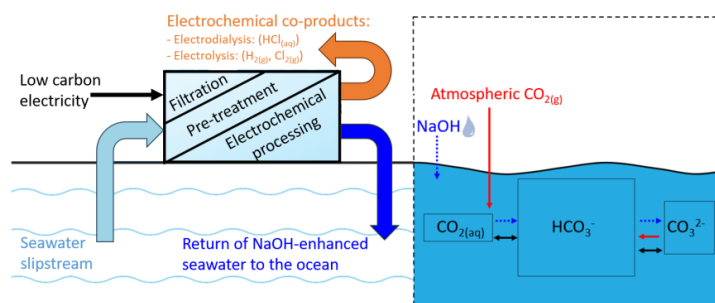
43 1 Introduction

44 The Sixth Assessment Report of the Intergovernmental Panel on Climate Change reported that in addition to a
45 drastic decrease in CO₂ emissions, active removal of 5.5 Gt of atmospheric CO₂ per year by 2100 is necessary to
46 constrain average global warming to less than 1.5 - 2 °C (IPCC, 2022; Rogelj, 2018). A wide variety of negative
47 emissions technologies (NETs) are under development to meet this enormous challenge (Minx et al., 2018;
48 NASEM, 2019; NASEM, 2022; Rueda et al., 2021; Vitillo et al., 2022).

49 A suite of promising approaches to CO₂ removal termed ocean or marine carbon dioxide removal (ocean CDR or
50 mCDR, respectively) leverage the enormous surface area and carbon storage capacity of the ocean (Boettcher et al.,
51 2019; NASEM, 2021). Ocean alkalinity enhancement (OAE) is an mCDR method that aims to store atmospheric
52 CO₂ in a dissolved phase in the ocean as bicarbonate ions (HCO₃⁻), thereby accelerating a natural planetary CO₂
53 regulation mechanism, the carbonate-silicate cycle (Berner, 1983; Isson et al., 2020). OAE has the potential to scale
54 to gigatons of CO₂ removal per year (He and Tyka, 2023), but development of this approach requires careful
55 consideration of: the methods and materials used to source and process alkalinity; the form and method of delivery
56 of alkalinity to the surface ocean (for example, aqueous or solid phase); and selection of appropriate geographic sites
57 for alkalinity dispersal (Oschlies et al., 2023). OAE methods under exploration include: mining and crushing
58 alkaline minerals (e.g., olivine, basalts) to be spread via ship or in coastal environments (e.g., beach restoration, or
59 salt marsh distribution) (Feng et al., 2017; Köhler, Hartmann, and Wolf-Gladrow, 2010; Monserrat et al., 2018;
60 Rigopoulos et al., 2018); the mining or industrial production of Mg(OH)₂ or mining CaCO₃ and calcining it to CaO
61 or Ca(OH)₂, with the Mg(OH)₂ or Ca(OH)₂ spread via ship or coastal outfall pipe (Harvey, 2008; Ilyina et al., 2013;
62 Kheshgi, 1995; La Plante, 2023; Moras et al., 2022; Nduagu, 2012; Rau, 2008; Renforth and Henderson, 2017;
63 Shaw, 2022); and the electrochemical conversion of saltwater into aqueous hydroxides and dispersal via coastal
64 outfalls (de Lannoy et al., 2018; Eisaman et al., 2018; Lu et al., 2022; Tyka, Van Arsdale, and Platt, 2022; Eisaman
65 et al., 2023).

66 Many of these approaches and technologies are at a nascent stage and we must move quickly to quantitatively test
67 and characterize their performance to determine which, if any, justify larger-scale deployment. The electrochemical
68 conversion of salt (NaCl) into aqueous alkalinity (NaOH) has many potential advantages in scaling considerations,
69 including simplified distribution of a liquid product to the ocean, avoidance of mining and the transportation of the
70 alkalinity source over long distances, and avoidance of potentially harmful impurities present in mined alkalinity
71 sources (NASEM, 2021; Caserini, Storni, and Grosso, 2022).

72 Figure 1 summarizes a specific OAE approach in which electrochemical processing of seawater or brine rearranges
73 the hydrogen (H⁺), hydroxide (OH⁻), sodium (Na⁺), and chloride (Cl⁻) ions to produce acidic (HCl) and basic
74 (NaOH) solutions. From a molecular point of view, since the Na⁺ and OH⁻ ions come from the seawater itself, the
75 net result of this process is the removal of H⁺ and Cl⁻ ions from the input seawater, that is the removal of HCl acid.
76 Nothing new is added to the ocean in this process, but rather H⁺ and Cl⁻ ions are removed from seawater.





78 **Figure 1:** Low-carbon electricity and a slipstream of seawater are the inputs to electrochemical OAE. Various
79 process-specific filtration and pretreatment steps allow for membrane-based electrochemical processing, resulting in
80 the removal of H^+ and Cl^- ions from seawater. The NaOH-enhanced seawater is returned to the ocean, resulting in
81 the invasion of CO_2 into seawater and durable storage as mostly HCO_3^- and some CO_3^{2-} .

82 In the process shown in Fig. 1, a portion of the salt (NaCl) in the seawater is electrochemically separated into its
83 constituent acid (HCl) and base (NaOH). The acid is removed, but the base is remixed with the seawater enhancing
84 the alkalinity of the resulting seawater that is then returned to the ocean. In the case where bipolar membrane
85 electrodialysis is used to generate the acid and base, water (H_2O) is dissociated into H^+ and OH^- ions at the junction
86 of the bipolar membranes inside the electrochemical system (Eisaman et al. 2012). This operation alone does not
87 change the alkalinity. But a voltage applied across a stack of ion-selective membranes then separates the H^+ and OH^-
88 ions from each other and from the seawater, with Cl^- ions (in HCl) and Na^+ ions (in NaOH) providing the charge
89 balance. Remixing the NaOH with the seawater but retaining the HCl results in a treated seawater solution an
90 increased OH^- concentration $[OH^-]$ compared to the input seawater.

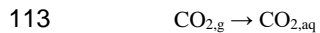
91 Total alkalinity (TA) is defined as the excess of proton acceptors over proton donors in an aqueous solution (Eq. 1),
92 where ellipses represent neglected acids and bases (Dickson 1981; Dickson 1992; Wolf-Gladrow et al., 2007). A
93 higher TA value for a seawater sample indicates that it has a higher buffering capacity than a sample with a lower
94 TA value. That is, for sample with a higher TA value, the addition of a given amount of acid to the sample will
95 decrease its pH less than for a sample with a lower TA value.

$$96 \quad TA = [HCO_3^-] + 2 [CO_3^{2-}] + [B(OH)_4^-] + [OH^-] + [HPO_4^{2-}] + 2 [PO_4^{3-}] + \dots - [H^+] - [HSO_4^-] - \dots \quad (1)$$

97 From Eq. (1), we see the increased OH^- concentration in a treated seawater solution corresponds to a salt solution
98 with increased alkalinity relative to the starting salt solution. The reason that the H^+ concentration remains the same
99 even though H^+ ions were removed is that both the H^+ and OH^- started as bound in an H_2O molecule, which was
100 then dissociated into free H^+ and OH^- ions at the bipolar membrane junction. Therefore, upon removing the H^+ ions
101 but remixing the OH^- ions, the H^+ ion concentration is the same as prior to H_2O dissociation, while the OH^- ion
102 concentration is increased. This increase in OH^- ion concentration rapidly increases the seawater pH upon mixing,
103 resulting in a shift of the dissolved inorganic carbon (DIC) speciation towards carbonate (Eisaman et al., 2023):



106 The concentration of dissolved CO_2 gas ($CO_{2,aq}$) in this alkalinity-enhanced seawater is less than it would be if it
107 were in equilibrium with atmospheric CO_2 (Equation 2b). Over the longer timescale required for air-sea gas
108 exchange - weeks to months (Wang et al., 2023) or months to years (He and Tyka, 2023) depending on location - the
109 disequilibrium in the surface ocean resulting from the alkalinity addition drives the invasion of atmospheric CO_2
110 into seawater (or lessens the outgassing of CO_2 from the surface ocean to the atmosphere), where it reacts with
111 carbonate and is stored primarily in the stable bicarbonate phase (Jones et al., 2014; Bach et al., 2023; Renforth and
112 Henderson, 2017; Eisaman et al., 2023).



116 Once equilibrium has been reached, the net reaction can be written as equation 4 (Eisaman et al., 2023):





118 where the coefficients a-e depend on seawater properties such as temperature, pressure, and pH through the
119 dependence of the equilibrium constants on these variables. Under typical ocean conditions, after equilibrium has
120 been reached, OAE results in an increase in the DIC in seawater on the order of 0.7-0.9 moles of DIC per mole of
121 NaOH added, with a slightly increased pH relative to the initial value (He and Tyka, 2023). For common surface
122 ocean conditions (e.g., 20°C, salinity 35, and initial TA of 2000 $\mu\text{mol kg}^{-1}$) at complete equilibrium, calculated
123 values of $a=0.84$, $b=0.71$, $c=0.13$, $d=0.002$, $e\approx 1$ can be obtained, which would correspond to 0.84 moles of DIC per
124 mole of NaOH.

125 It is possible that air-sea gas exchange will not completely drive the seawater $p\text{CO}_2$ to the initial unperturbed value
126 before the seawater sinks into the ocean interior and loses contact with the atmosphere for hundreds to thousands of
127 years. Therefore, the DIC anomaly relative to the alkalinity anomaly present when the seawater sinks into the ocean
128 interior may be used to assess the effective impact of the OAE for capturing atmospheric CO_2 on the 0-100 year
129 timescales that are most important for climate interventions.

130 In addition to the storage of atmospheric CO_2 in the form of DIC, this process may have the potential to locally
131 mitigate ocean acidification. In a water body with a finite seawater exchange rate with the ocean, such as a semi-
132 protected estuary or bay, alkalinity could be added in a controlled manner such that the combination of the rapid
133 reactions described by Eq.(1) and the exchange/flushing rate with the open ocean result in the bay being held in
134 steady-state at a target pH or aragonite saturation state value that is higher than its equilibrium value under
135 conditions of ocean acidification. As this added alkalinity diffuses through the bay and makes its way to the open
136 ocean, CO_2 removal and storage as DIC would occur. Even once equilibrium has been achieved, the pH and the
137 carbonate ion concentration in the open ocean remains slightly higher than before the alkaline discharge. By
138 metering the rate of alkalinity addition to the bay to match the flushing rate, the pH or saturation state of the bay can
139 be held at a constant target value. We refer to this approach as the SEA MATE process: the Safe Elevation of
140 Alkalinity for the Mitigation of Acidification Through Electrochemistry.

141 Deploying SEA MATE in the ocean or coastal waters will require an understanding of carbonate chemistry in
142 seawater in the ocean volume under consideration, as well as thresholds for safe operation. For example, at the point
143 of alkaline dispersal where there is the maximum change in seawater chemistry, SEA MATE must control the rate of
144 alkalinity addition relative to the rate of mixing and dilution in the ocean to avoid the precipitation of $\text{Mg}(\text{OH})_2$ or
145 CaCO_3 (Hartmann et al., 2023; Moras et al., 2022). While $\text{Mg}(\text{OH})_2$ readily redissolves, an increase in turbidity due
146 to precipitation may negatively affect marine organisms (Bainbridge et al., 2018; Broderson et al., 2017; Dutertre et
147 al., 2009). By contrast, CaCO_3 will generally not redissolve in the surface ocean without biological mediation, and
148 runaway precipitation, where alkalinity removed by precipitation exceeds that added by the OAE treatment, can
149 occur under conditions of increased aragonite saturation state and increased nucleation sites in the water column
150 (Moras et al., 2022). CaCO_3 precipitation could counteract the intended effect of the OAE intervention by removing
151 alkalinity from the surface ocean and releasing CO_2 gas via Eq. 5 (Zeebe and Wolf-Gladrow, 2001):



153 Upon dispersal to the ocean through a coastal outfall pipe, the added alkalinity is advected and diffuses away from
154 the point source, becoming increasingly diluted through the mixing zone. Because the timescale for air-sea gas
155 exchange and re-equilibration described by Eq. (2) is longer than the characteristic timescale for dilution driven by
156 tides, currents, and weather, most of the CO_2 removal occurs far from the mixing zone. Dilution will spread the
157 impacts over a broad area, to an extent that it is unlikely that the impacts on the DIC distribution can be quantified
158 using only direct measurements, given current instrument resolution and the typical dynamic range of natural
159 variability (Wang et al., 2023). In general, options for measurement, reporting, and verification (MRV) of OAE will
160 therefore rely on (Ho et al., 2023): experimentation in laboratory and mesocosm settings, such as the work we
161 describe here, to establish CO_2 removal dynamics under conditions of OAE; direct monitoring of the rate and



162 characteristics of alkalinity addition into seawater; monitoring the seawater carbonate and environmental chemistry
163 in the immediate vicinity of the outfall via sensors and sampling (Cyronak et al., 2023; Schulz et al., 2023); and
164 ocean modeling to estimate CDR beyond the range of direct detection (Fennel et al., 2023).

165 While some work has investigated various aspects of NaOH-based ocean alkalinity enhancement in microcosms
166 (Ferderer et al., 2022; Hartmann et al., 2023), in mesocosms (Groen et al., 2023), and over natural coral reefs
167 (Albright et al., 2016), a systematic characterization of the efficiency and kinetics of OAE as a function of key
168 process parameters has not yet been performed. Here we report the first tank-scale tests of OAE that use aqueous
169 hydroxide (NaOH) to enhance the alkalinity of natural seawater, a process that mimics OAE via the electrochemical
170 brine-to-alkalinity conversion used in the SEA MATE process. Our experiments, conducted in 6,000 liter tanks
171 using seawater pumped from Flax Pond on Long Island Sound in Stony Brook NY, quantify the magnitude and
172 timescale of the CO₂ removal from the air and storage as seawater DIC by monitoring the air-seawater re-
173 equilibration after an initial alkalinity perturbation. In addition, our use of both laboratory-processed bottle samples
174 and field-deployable sensors to measure and over-constrain the carbonate chemistry response allows us to assess the
175 suitability of certain sensing platforms for MRV. Finally, we investigate safe thresholds for the rate and
176 concentration of alkalinity addition to avoid: (1) the precipitation and redissolution of Mg(OH)₂ that can lead to
177 local, temporary increases in turbidity; and (2) the precipitation of CaCO₃, which partially reverses the intended
178 OAE effect by removing alkalinity from, and releasing CO₂ gas into, the surrounding seawater.

179 Using this approach, we address the following key questions:

180 (1) How much additional atmospheric CO₂ is stored in seawater as DIC in response to a given alkalinity
181 perturbation?

182 (2) What is the timescale for CO₂ removal from the air, and how does it depend on pH and the magnitude of
183 alkalinity enhancement?

184 (3) If Mg(OH)₂ precipitates upon addition of NaOH to seawater, on what spatial and temporal scales does it
185 redissolve?

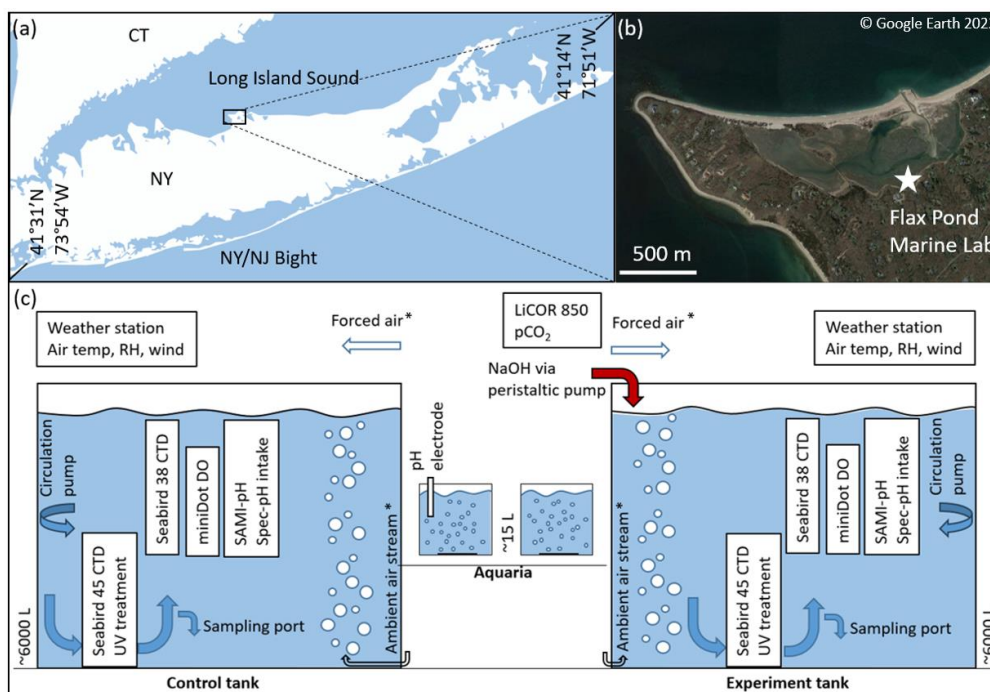
186 (4) What are the threshold values for pH and aragonite saturation state beyond which undesired CaCO₃ precipitation
187 will occur?

188 Answering these questions is key to assessing the viability of this approach and to optimizing its eventual
189 deployment.

190 **2. Methods**

191 **2.1 Experimental procedure**

192 We investigated the carbonate chemistry changes resulting from the addition of NaOH_(aq) to natural seawater over
193 timescales ranging from 2 weeks to 2 months in a series of experiments at two scales: (1) two large (~6200 L)
194 indoor tanks, and (2) multiple 15 L aquaria (Fig. 2).



195

196 **Figure 2:** (a, b) Flax Pond Marine Laboratory is located on Long Island Sound, New York, USA (© Google Earth
197 2022). (c) The ~6000 L control and experiment tanks were instrumented with a series of oceanographic sensors and
198 sampled routinely for DIC/ TA analyses to allow for measurement of carbon uptake over time following an addition
199 of alkalinity in the form of NaOH. The ~15 L aquaria were instrumented with standard pH electrodes and monitored
200 with routine TA analyses. The Forced air* and Ambient air streams* indicate their use in some but not all
201 experiments, as noted in later sections.

202 This study was conducted at the Flax Pond Marine Laboratory at Stony Brook University, NY. All experiments used
203 natural seawater collected from Flax Pond, part of a 128-acre salt marsh tidal wetlands connected to the Long Island
204 Sound. The surface areas of the tanks and aquaria were ~4.6 m² and ~0.1 m², respectively. The tanks had a diameter
205 of 0.24 m, a total height of 1.52 m, and were typically filled to a height of ~1.35 m, allowing for a corresponding
206 seawater volume of 6185 L. The large tank volumes were chosen to limit interactions with walls while increasing
207 the air-seawater boundary, and to allow for in-situ oceanographic sensor deployment and frequent bottle sampling
208 while retaining semi-controlled temperature, mixing, filtration, and biological control. The inherent limitations of
209 these tank tests include limited air-sea interaction, unrealistic light levels and circulation, and biological responses
210 that are not a perfect representation of natural seawater in the ocean, but serve as a stepping stone to mesocosm and
211 eventual field experiments. On average, the large (~6,000 L) tank experiments took ~6.5 weeks after dosing with
212 NaOH to reach 90% of the calculated or extrapolated asymptotic Δ DIC/TA addition ratio indicative of full air-
213 seawater equilibrium, as will be discussed in Section 3. Therefore, in addition to the large tank tests, we conducted a
214 series of smaller aquaria alkalinity additions to increase our capacity for experimental test cases. The limitations of
215 the aquaria include limited sensor options, unrealistic circulation, and limited biological control.

216 2.1.1 Tank experiments



217 Seawater was pumped into the tanks at high tide through a series of sock filters to exclude macroscopic biology. The
218 tanks were then dosed to 40 ppm bleach (sodium hypochlorite) and the shock-treated seawater was allowed to
219 circulate through the tanks for ~1 day to limit biological growth. The seawater was then circulated through UV light
220 arrays to break down the bleach over ~1-2 weeks, as assessed by a standard Hach test kit for free chlorine. During
221 this period, seawater was pumped between the two large test tanks (~25 L/min) to increase mixing of the bleach and
222 to homogenize the tanks to similar initial conditions. For the remainder of each experiment, the seawater was
223 continually pumped through the UV sterilizers.

224 Oceanographic sensors and discrete daily bottle sampling, as described in Sections 2.2 and 2.3, respectively, were
225 deployed for carbonate chemistry analysis for several days prior to the alkalinity addition to understand the initial
226 baseline conditions in both tanks. Two submerged pumps were used for water circulation within each tank: the first
227 pump (Current eFlux DC Flow Pump, 210 GPH) cycled seawater through the UV arrays with an estimated
228 overturning time of the bulk tank on order of 1 day, and a second (Kedsum Submersible pump, 260 GPH), mounted
229 at an angle halfway down the tank wall, allowed for subsurface circulation within the tank to reduce the occurrence
230 of unmixed ‘dead zones’ and subsequent non-homogenous biological growth, as assessed visually on the surface of
231 the water and/or tank lining. With exceptions discussed in Section 2.4, the surface of each tank was still throughout
232 the experiments.

233 After baselining, one tank (referred to as the “experimental tank”) was dosed with enough 0.5 M NaOH (see
234 Supplementary Materials) to raise the bulk seawater pH to the target pH of interest for a given experiment, and the
235 same volume of DI water was added to the other tank (referred to as the “control tank”). NaOH additions were
236 typically dosed into the tank via peristaltic pump at a low enough rate (~50 mL/min) that a steady increase in bulk
237 tank pH was observed, but local pH measured just below the NaOH introduction never exceeded a pH of 9.0. A
238 pump (~25 L/min) was placed just below the NaOH stream to speed the mixing of NaOH into the bulk tank,
239 increase dilution from the point source, and to prevent the immediate precipitation of $Mg(OH)_2$ upon contact of the
240 NaOH with seawater. This pump was removed after the full volume of NaOH was mixed into the tank.

241 After the alkalinity addition, the tanks were left to equilibrate with the atmosphere and were monitored by sensors
242 and sampling as described in Sections 2.2 and 2.3. The tanks were indoors in the wet laboratory at Flax Pond Marine
243 Lab, such that temperature and CO_2 concentration were moderated by the building’s HVAC system, but varied
244 throughout days and seasons depending on other uses of the lab space. The experiments were concluded when the
245 observed pH or DIC (calculated from daily pH and frequent TA measurements) appeared to stabilize (e.g., ΔpH
246 $\pm 0.05\%$ or $\Delta DIC \pm 10 \mu mol kg^{-1}$ per day) over several days. The continuous improvement of experimental methods
247 during this study resulted in some minor variations among the methods used for each experiment, including methods
248 of NaOH dosing, tank circulation, and biological control, as discussed where necessary in Section 3 and in the
249 Supplementary Materials.

250 2.1.2 Aquaria experiments

251 A series of polycarbonate aquaria were filled with 15 L of seawater taken from the large control tank just after the
252 described bleaching and bleach breakdown procedure was completed. NaOH was dosed into each aquaria to reach a
253 targeted bulk pH_T , with a corresponding volume of DI H_2O added to the control aquaria, and then the seawater was
254 allowed to equilibrate with atmospheric pCO_2 over days to weeks. The aquaria did not have either UV light arrays
255 for biological control or aquarium pumps for internal circulation. In most cases, the aquaria were bubbled with air
256 (~4 L/min) via a standard aquarium bubbling bar spanning the center diameter of each aquarium to reduce the
257 equilibration time of these experiments compared to the large tank experiments for all initial pH conditions
258 investigated. No sensors were deployed in the aquaria due to their limited size, and seawater chemistry was
259 established via discrete pH_T and TA measurements (Sect. 2.2).



260 As shown in Eq. (6), we define the dimensionless ‘Carbon-to-Alkalinity Ratio’ (CAR) for our experiments as the
261 molar ratio of the increase in $n\text{DIC}$ (in units of $\mu\text{mol/kg}$, normalized to the system’s initial salinity to account for
262 evaporation) to the magnitude of the TA increase (ΔTA , in units of $\mu\text{mol/kg}$). $n\text{DIC}_{\text{equ}}$ is the measured (via direct
263 titration) or calculated (via CO2SYS using measured TA and pH_T) DIC value that the system reached at the end of
264 an experiment (Pierrot et al., 2006; Van Heuven et al., 2011). Some experiments were left long enough to achieve
265 equilibration with atmospheric CO_2 , but others were halted early. In these cases, a CO2SYS calculation was used to
266 estimate the DIC increase expected at equilibration given initial seawater conditions, and the difference between this
267 value and the final recorded $n\text{DIC}_{\text{equ}}$ was used to estimate the overall percent equilibration for a given experiment.
268 Depending on experimental constraints described in later sections, $n\text{DIC}_i$ may represent either: (1) the final $n\text{DIC}$
269 measured (via titration of bottle samples) or calculated (via CO2SYS using seawater TA and pH) in the control tank,
270 or (2) the ‘baseline’ $n\text{DIC}$ before the addition of NaOH to a given aquaria experiment, for cases where a
271 corresponding control case may not be available. Note that because we are reporting CAR values where the
272 measured DIC has reached or has been estimated at equilibrium, the CAR values we measure and report reflect the
273 ratio of ΔDIC to ΔTA that would be expected given sufficient time for air-sea exchange to reach equilibrium, and so
274 are equivalent to directly measuring the value of the “TA addition potential impact ratio” as defined by Wang et al.,
275 2023.

$$276 \quad \text{Carbon-to-Alkalinity Ratio (CAR)} = (n\text{DIC}_{\text{equ}} - n\text{DIC}_i) / \Delta\text{TA}$$

277 (6)

278 2.2 Oceanographic sensors

279 Each tank was instrumented with a series of sensors placed halfway down the wall of the tank near the inlet of the
280 UV circulation pump. A Seabird 38 Digital Oceanographic Thermometer and Seabird 45 MicroTSG
281 Thermosalinograph continuously monitored seawater temperature and salinity, respectively. Dissolved oxygen was
282 measured by a PME miniDOT Logger at 10 min resolution. pH_T was monitored daily by a SAMI-pH (manufacturer
283 specified accuracy/precision $\sim 0.003/0.001$, though this accuracy is likely an underestimate of the uncertainty given
284 known challenges for the calibration of the pH_T measurements) and by a semi-automated spectrophotometric (spec-
285 pH) pH unit ($\sim \pm 0.0055/0.0004$) as described by Carter et al. (2013). CRM measurements were taken by each pH
286 system at the beginning and end of each experiment and were used alongside discrete samples of DIC and TA as
287 described in Section 2.3 to constrain the stability of each sensor. The SAMI-pH measurements were recorded at
288 ambient seawater temperature and corrected for in-situ salinity as recorded by the Seabird Thermosalinograph
289 following best practices from the manufacturer. The spec-pH analyses occurred in a jacketed cuvette held at 20°C
290 (regulated via water bath) and were corrected to the in-situ bulk tank temperature and salinity as recorded by the
291 Seabird Thermometer and Thermosalinograph. Both the SAMI-pH and spec-pH rely on spectrophotometric analysis
292 of metacresol purple indicator dye, which allows for pH measurement within the pH_T range of approximately 7 to 9.
293 For experiments in which enough NaOH was dosed into seawater to raise pH above these limits, a Thermo Scientific
294 Orion ROSS Ultra pH/ATC Triode combination electrode (8157BNUMD) was used to monitor pH_{NBS} at the surface
295 of the tank (± 0.01 precision), which was then converted to pH_T for comparison with the other pH sensor systems.

296 A LiCOR LI-850 sensor was used to analyze atmospheric $p\text{CO}_2$ ($\pm 1.5\%$ accuracy) above the tanks. The inlet to this
297 sensor was periodically moved between tanks to ensure that atmospheric $p\text{CO}_2$ in the vicinity of the control and
298 experiment tanks was the same. AcuRite Iris weather stations were mounted on the side of each tank to monitor air
299 temperature ($\pm 2^\circ\text{C}$), relative humidity ($\pm 3\%$), and air speed ($\pm 0.8 \text{ m s}^{-1}$). All data were compiled on an hourly basis
300 in a custom R package.

301 2.3 Discrete sampling



302 Two types of discrete sampling were used to constrain carbonate chemistry throughout these experiments. First, 500
303 mL of seawater was collected and preserved from each tank, typically on a daily basis, and as frequently as hourly
304 during the addition of NaOH, following best practices laid out by Dickson (2007) including overflowing of the
305 sample bottles during collection and addition of 0.2 mL of saturated mercuric chloride (HgCl_2) as a preservative.
306 These bottle samples were analyzed for DIC and TA at NOAA Pacific Marine Environmental Laboratory
307 (NOAA/PMEL). DIC concentrations were measured using a coulometer (UIC Inc.) and Single Operator
308 Multiparameter Metabolic Analyzer (SOMMA) (Johnson et al., 1985; 1993). TA was determined by an open-cell
309 acidimetric titration (Dickson et al. SOP 3b, 2007). The accuracy of DIC and TA measurements was assessed with
310 Certified Reference Materials (CRMs, supplied by the Dickson laboratory at Scripps Institution of Oceanography),
311 and overall uncertainty for both DIC and TA was typically $\pm 0.1\%$ ($\sim 2 \mu\text{mol/kg}$).

312 In addition, discrete seawater samples were analyzed for TA via open-cell potentiometric titration at Stony Brook
313 University. A Thermo Scientific Orion ROSS Ultra pH/ATC Triode combination electrode (8157BNUMD),
314 calibrated using three buffer solutions (pH_{NBS} 4.01, 7, and 10.01) was used to track the titration of a ~ 20 mL
315 seawater sample with a dilute HCl solution (~ 0.1 M in 0.7 M NaCl, calibrated daily with CRM or a secondary
316 seawater standard) following a modified Gran titration procedure using a Kloehe digital syringe pump (Song et al.,
317 2020; Wang and Cai, 2004). The precision of TA measurements was $\sim \pm 5$ -10 $\mu\text{mol/kg}$. This TA data was corrected
318 to that of the bottle samples analyzed via titration at NOAA PMEL where available (see Supplementary Materials).

319 There are several differences between the aquaria experiments and the larger tank experiments. First, the aquaria
320 experiments were monitored daily to every few days by discrete measurement of TA at Stony Brook University and
321 pH_{NBS} via Thermo Scientific Orion ROSS Ultra pH/ATC Triode combination electrode (8157BNUMD) (± 0.01
322 precision), which was then converted to pH_{T} and corrected against the other pH sensor systems via occasional bottle
323 samples for DIC and TA analysis at NOAA PMEL. Variations between these experiments are noted in Section 3
324 where necessary and in the Supplementary Materials.

325 In either tank or aquaria cases where mineral precipitation was observed, 0.5 – 1 L of seawater was vacuum filtered
326 through a 0.45 μm Whatman GF/F filter via vacuum pump and the solids were rinsed with DI water 3 times to
327 remove NaCl. The precipitate was dried in an oven at 90 °C, then crushed into a uniform powder via mortar and
328 pestle. Samples were analyzed via Hitachi 4800 Scanning Electron Microscopy (SEM) (5 kV) and Rigaku SmartLab
329 X-ray Diffraction (XRD) ($\text{Cu K}\alpha$, 1.5406 Å, 10 - 100° 2 θ at 4°/min) at Brookhaven National Laboratory at the
330 Materials Synthesis and Characterization Facility of the Center for Functional Nanomaterials.

331 **2.4 Evaluation of CO₂ uptake by seawater in response to NaOH perturbation**

332 Seawater carbonate chemistry measurements were used to analyze the uptake of CO₂ in each tank, primarily relying
333 on calculations from the NOAA/PMEL DIC and TA analyses of bottle samples when available and using sensor pH
334 and Stony Brook TA measurements for cross-verification or to fill in between discrete DIC samples. Carbonate
335 chemistry calculations were performed using CO2SYS (Lewis and Wallace, 1998), with Leuker et al. (2000)
336 carbonate constants, Dickson (1990) for KSO_4 , and Lee et al. (2010) for total boron. Wherever possible, a
337 combination of CRM analyses and comparisons between simultaneous pH sensor and NOAA PMEL bottle samples
338 were used to correct SAMI-pH and spectrophotometric pH sensor data for drift. DIC and TA data were normalized
339 to the salinity at the start of a given experiment to account for evaporation (Friis et al., 2003).

340 Changes in the seawater carbonate chemistry over time were analyzed with respect to shifts away from the baseline
341 within a single control or experiment tank, as well as with respect to the differences between the control and
342 experimental tanks.

343 **3 Results and Discussion**



344 3.1 Large tank experiments

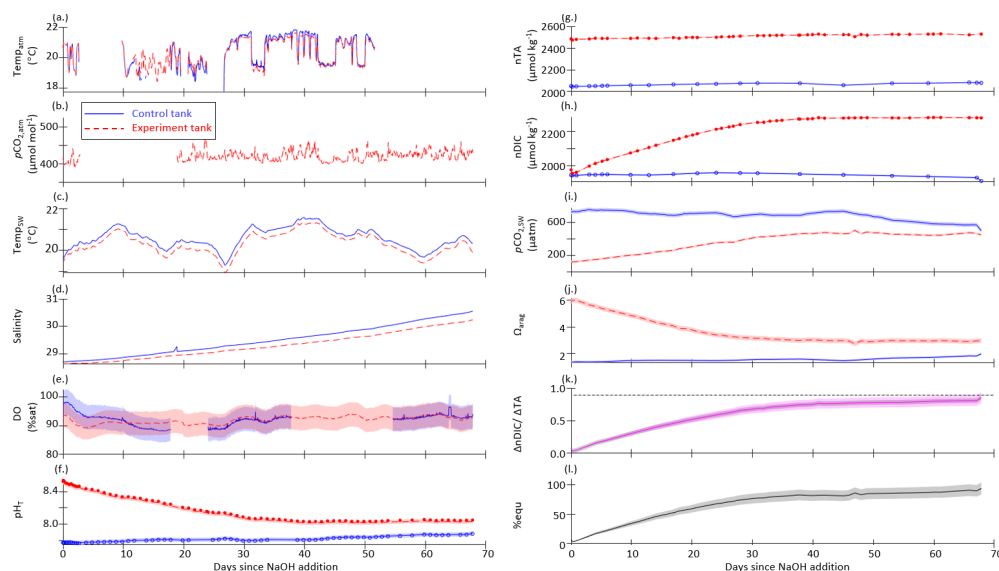
345 A summary of the range of oceanographic variables measured by sensors and bottle samples, calculated via
346 CO2SYS, or extrapolated to equilibration conditions during the large tank experiments is provided in Table 1. This
347 summary includes 6 experiments including 3 targeting pH_T 8.5 (still surface water, with forced air, and with forced
348 air and air bubbling) and one (each) targeting pH_T values of 8.7 (still surface water), 9.5 (with forced air and air
349 bubbling), and 10.3 (still surface water). In two early experiments in which bulk pH_T was raised from the initial
350 condition to 8.3 and to 8.7, the initial pH_T and TA varied between the control and experiment tanks as seawater was
351 pumped from multiple reservoirs and unevenly distributed between the tanks. The experiments were subsequently
352 refined to allow for several days of cross-pumping between tanks to homogenize the control and experiment
353 seawater before NaOH was added at the start of an experiment. More details on experimental variations and a larger
354 summary table are available in the Supplementary Materials.

355 The initial pH_T , TA, and DIC varied across experiments as seawater was collected between March 2022 and May
356 2023, ranging from pH 7.66 (December 2022) – 7.95 (May 2023), TA 2001 (May 2023) – 2176 (March 2023)
357 $\mu\text{mol/kg}$, and DIC 1847 (May 2023) – 2021 (March 2023) $\mu\text{mol/kg}$. Both measured and CO2SYS -calculated DIC
358 and TA values were normalized to salinity to account for evaporation, which drove salinity increases ranging from
359 0.2 – 7.1 across these experiments.

360 After the addition of NaOH, the control and experiment tanks were allowed to equilibrate with atmospheric CO_2 .
361 While refinements in the experimental design allowed for complete or near-complete equilibration in later
362 experiments, as determined by the stabilization of nDIC at some asymptotic value, early experiments were
363 terminated before full equilibration. In all experiments, the absorption of atmospheric CO_2 began immediately after
364 the NaOH addition, as determined by decreasing pH and Ω_{arag} and increasing DIC and seawater $p\text{CO}_2$. nTA was
365 fairly stable or increasing (+10 - 60 $\mu\text{mol kg}^{-1}$) after the NaOH addition in all cases except the $pH_T = 10.3$
366 experiment, where nTA and DIC rapidly decreased due to runaway CaCO_3 precipitation. A stable TA value is an
367 indicator that no significant persistent mineral precipitation (e.g., $\text{Mg}(\text{OH})_2$ or CaCO_3) has occurred. In the absence
368 of active mixing or bubbling, $\text{Mg}(\text{OH})_2$ precipitation occurred immediately upon the introduction of NaOH to
369 seawater, however the precipitation can be rapidly dissolved by turbulence (i.e., pumping NaOH directly above a
370 strong circulation pump and/or stream of air bubbles). No CaCO_3 precipitation was observed in the tanks or aquaria
371 for which the bulk seawater pH_T was <10.0 . The $pH_T = 10.3$ experiment was designed to induce CaCO_3 runaway
372 precipitation, as described in Section 3.3.

373 Ω_{arag} ranged from 1.4 - 2.5 in the control tanks with minimal variation over the course of any given experiment.
374 During the three experiments in which bulk pH_T was increased to ~ 8.5 , Ω_{arag} increased immediately to 6.0 - 6.3 at the
375 peak of the experiments, before slowly decreasing to 2.8 - 3.0 as the seawater equilibrated with atmospheric CO_2 .
376 For the bulk pH_T 9.5 experiment, Ω_{arag} increased to 20.2 and slowly decreased to 5.0 when the experiment was
377 ended at full equilibration. Mineral precipitation was observed in the bulk pH_T 10.3 experiment, where Ω_{arag} was
378 increased to 30.3 and rapidly (<1 week) fell to 5.2 after the addition of NaOH.

379 The results of one representative set of time-series measurements from the control and experiment tanks are shown
380 in Figure 3 for the case where pH_T of the bulk experiment tank was raised to 8.5 then allowed to relax into
381 equilibration with the atmosphere without the addition of surface air forcing or bubbling. Time-series plots for the
382 other tank-scale experiments are available in the Supplementary Materials.



383

384 **Figure 3:** Time-series data for the case where pH_T of the bulk experiment tank was raised to 8.5 with no forced air
 385 flow and no bubbling (still surface) for control (blue, solid) and experiment (red, dashed) tanks: (a) continuously
 386 measured air temperature, (b) atmospheric $p\text{CO}_2$, (c) seawater temperature, (d) salinity, and (e) dissolved oxygen; (f)
 387 pH_T measured by the SAMI-pH (circles) and interpolated from the spec-pH (line), corrected to bottle sample and
 388 CRM data; (g) NOAA/PMEL-measured TA and (h) DIC from bottle samples and normalized to salinity; (i)
 389 seawater $p\text{CO}_2$ and (j) saturation state of aragonite (Ω_{arag}) calculated from interpolated nDIC and nTA data via
 390 CO2SYS; (k) the observed carbon uptake ratio (CAR) as $(n\text{DIC}_{\text{exp}} - n\text{DIC}_{\text{control}}) / \Delta\text{TA}_{\text{NaOH addition}}$ (solid) and the
 391 theoretical CAR (dashed) from a CO2SYS calculation using measured TA and the average $p\text{CO}_2_{\text{atm}}$ to estimate the
 392 equilibrium change in DIC (dashed); (l) the percent equilibration estimated between the observed and theoretical
 393 CAR. Data gaps in panels a, b, and e are due to connectivity issues while offloading sensor data.

394 The $\Delta n\text{TA}$ and $\Delta n\text{DIC}$ values calculated between the control and experiment tanks are summarized in Figure 4,
 395 where nTA and nDIC were interpolated between bottle samples measured at NOAA-PMEL, and/or were calculated
 396 via CO2SYS using sensor pH_T and TA measured at Stony Brook University corrected to less frequent NOAA-
 397 PMEL TA and DIC bottle samples. The ratio of the $\Delta n\text{DIC}$ to the addition of alkalinity in the form of NaOH, or
 398 $\Delta n\text{TA}$, is included in Figure 4 for all experiments except that of the bulk pH_T increase to 10.3. Neglecting
 399 experiments that were terminated before full equilibration, the final observed CAR ranged from 0.75 ± 0.04 to 0.87
 400 ± 0.08 (Table 1).

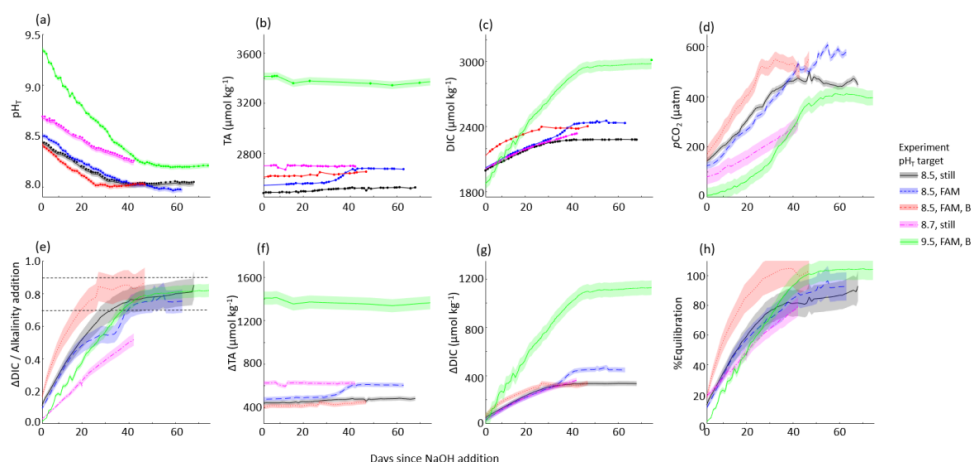
401 Henry's law and CO2SYS calculations were used to estimate the initial and final equilibration condition of each
 402 tank experiment. LiCOR $p\text{CO}_2_{\text{atm}}$ measurements were averaged across experiments to a representative value of 421
 403 ± 14 ppm, which was used with the initial seawater temperature and salinity to estimate $p\text{CO}_2_{\text{seawater}}$ at the beginning
 404 of each experiment. This initial $p\text{CO}_2_{\text{seawater}}$ was in all cases greater than the atmospheric $p\text{CO}_2_{\text{seawater}}$, indicating
 405 that the seawater was not fully equilibrated with the atmosphere at the time when NaOH was added, likely due to
 406 respiration and decomposition of biology removed during the bleaching step (Section 2.1), and as such, the tanks
 407 should outgas CO_2 . The initial equilibrium DIC was estimated from a CO2SYS calculation using the $p\text{CO}_2_{\text{seawater}}$
 408 and $n\text{TA}_i$, which in all cases was less than the initial nDIC measured or calculated from $n\text{TA}_i$ and $\text{pH}_{T,i}$ (by $29 - 108$
 409 $\mu\text{mol kg}^{-1}$). These observations underscore the importance of having a control tank to capture natural dynamics of
 410 CO_2 ingassing and outgassing to ensure that changes in DIC attributed to OAE are correctly accounted for.



411 The final equilibrium $n\text{DIC}$ was estimated from a CO2SYS calculation using the same $p\text{CO}_{2,\text{seawater}}$ and the $n\text{TA}$
 412 measured just after the NaOH addition, corrected for the linear increase in salinity over the course of the experiment.
 413 The ratio of the expected $\Delta n\text{DIC}$ calculated at equilibrium with the atmosphere to the addition of alkalinity provides
 414 a simple estimate of the expected CO_2 storage capacity for a given experiment. The percent equilibration for each
 415 experiment was then estimated from the measured and expected values for CAR. Within the series of experiments
 416 with a targeted pH_T of 8.5, the timeline to reach an estimated 90% CO_2 equilibration decreased from 65 days (with
 417 internal circulation but still water at the surface of the tank), to 50 days (with the addition of forced air movement
 418 across the surface of the tank) to 22 days (with the addition of air bubbling). We note that only the two cases
 419 (targeted pH_T of 8.5 and 9.5) with the addition of air bubbling reached full equilibration with the atmosphere.

420 **Table 1:** Range of variables measured, calculated, or extrapolated in large tank experiments, where M denotes direct
 421 measurement, C denotes calculation via CO2SYS, and E denotes extrapolation to equilibrium conditions. Subscripts
 422 i and f refer to initial and final conditions, and ‘peak’ refers to the time point immediately after the addition of
 423 NaOH.

pH target	-	8.5		8.5		8.5		8.7		9.5		10.3	
Surface condition	-	Still		Forced Air		Forced Air and Air Bubbles		Still		Forced Air and Air Bubbles		Still	
Tank (C = control, E = experiment)	-	C	E	C	E	C	E	C	E	C	E	C	E
$\Delta\text{TA} = \text{NaOH}$ addition ($\pm 10 \mu\text{mol/kg}$)	M	0	409	0	462	0	375	0	626	0	1406	0	3305
Salinity _i (g/kg)	M	28.7	28.7	30.2	30.2	30.4	30.4	26.9	26.8	26.9	26.9	28.5	28.4
Salinity _f (g/kg)	M	30.5	30.2	37.3	36.6	34.7	33.7	27.6	27.6	29.0	29.2	28.6	28.6
$\text{pH}_{T,i}$ (± 0.005)	M	7.76	7.76	7.73	7.73	7.93	7.93	7.92	7.75	7.95	7.95	7.70	7.75
$\text{pH}_{T,\text{peak}}$ (± 0.005)	M	-	8.54	-	8.58	-	8.49	-	8.68	-	9.51	-	10.10
$\text{pH}_{T,f}$ (± 0.005)	M	7.88	8.05	7.85	7.99	7.99	8.01	7.84	8.26	8.01	8.21	7.75	9.52
$n\text{TA}_i$ ($\pm 10 \mu\text{mol/kg}$)	M	2049	2049	2069	2069	2248	2248	2075	2075	2007	2007	2023	2025
$n\text{TA}_{\text{peak}}$ ($\pm 10 \mu\text{mol/kg}$)	M	-	2458	-	2531	-	2623	-	2701	-	3414	-	5330
$n\text{TA}_f$ ($\pm 10 \mu\text{mol/kg}$)	M	2080	2528	2235	2674	2246	2624	2095	2696	2014	3363	2041	1253
$n\text{DIC}_i$ ($\mu\text{mol/kg}$)	M	1944	1947	1957	1996	2082	2087	1897	1975	1852	1852	1928	1938
$n\text{DIC}_f$ ($\mu\text{mol/kg}$)	M	1908	2280	2084	2433	2027	2365	1937	2336	1832	2977	1947	720
$\Omega_{\text{aragonite},i}$	C	1.39	1.37	1.4	1.1	2.0	2.0	2.4	2.4	1.9	1.9	1.4	1.3
$\Omega_{\text{aragonite},\text{peak}}$	C	-	5.9	-	6.0	-	6.2	-	8.8	-	19.3	-	30.3
$\Omega_{\text{aragonite},f}$	C	2.0	3.0	1.7	2.8	2.5	3.0	1.9	4.4	2.1	4.9	1.4	5.2
CAR_f	C	-	0.85 ± 0.04	-	0.75 ± 0.04	-	0.87 ± 0.08	-	0.52 ± 0.07	-	0.82 ± 0.09	-	-
$\text{CAR}_{\text{equilibrium}}$	E	-	0.89	-	0.85	-	0.85	-	0.84	-	0.81	-	-
% equilibration (time elapsed in days)	E	-	95 ± 10 (67)	-	92 ± 10 (63)	-	102 ± 12 (45)	-	79 ± 6 (42)	-	104 ± 7 (74)	-	(13)



424

425 **Figure 4:** Results of 5 tank-scale experiments in which enough NaOH was added to each tank to raise the bulk pH_T
 426 to 8.3 – 9.7. pH_T decreased rapidly in all cases in which air bubbling sped equilibration with atmospheric CO₂.
 427 Results include: (a) measured pH_T, (b) measured TA, (c) measured DIC or CO₂SYS calculated (for pH_T 9.5 case
 428 only), (d) CO₂SYS -calculated pCO₂, (e) the observed carbon uptake ratio (CAR) as $(DIC_{exp} - DIC_{control}) / \Delta TA_{NaOH}$
 429 addition with horizontal dashed lines representing the expected range of 0.7-0.9 mol CO₂ uptake / mol NaOH added to
 430 seawater, the change in (f) TA and (g) DIC compared to the baseline measurements before the addition of NaOH,
 431 and the percent equilibration estimated between the observed and theoretical CAR.

432 3.2 Aquaria experiments

433 The large volume of tank experiments allowed for precise measurement of the seawater carbonate chemistry via
 434 bottle sampling (1L each, sent to NOAA/PMEL for analysis) with high sampling frequency. To compliment these
 435 measurements, we also performed a series of experiments in smaller aquaria (15 L each), which enabled a larger
 436 number of replicates and a faster time to equilibrium when bubbled with air. Table 2 provides a summary of the
 437 range of oceanographic variables quantified for the aquaria experiments.

438 **Table 2:** Range of variables measured, calculated, or extrapolated in aquaria experiments, where M denotes direct
 439 measurement, C denotes calculation via CO₂SYS, and E denotes estimation within specified equilibration
 440 conditions. Subscripts *i* and *f* refer to initial and final conditions, and ‘peak’ refers to the time point immediately
 441 after the addition of NaOH.

pH target	-	0 Control	8.3	8.5	8.5 Without air bubbles	8.7	9.3	9.5	9.7	9.9	10.0	10.1	10.2	10.3
$\Delta TA = \text{NaOH}$ addition (± 10 $\mu\text{mol/kg}$)	M	0	187	331	362	543	1409	1679	2037	2216	2276	2504	2796	3829
pH _{T,i} (± 0.005)	M	7.94	7.97	7.90	7.86	7.95	7.98	7.98	7.98	8.06	8.04	8.04	8.04	7.95
pH _{T,peak} (\pm 0.005)	M	-	8.28	8.41	8.40	8.63	9.22	9.43	9.64	9.83	9.91	10.23	10.32	10.20
pH _{T,f} (± 0.005)	M	8.06	8.03	8.07	8.11	8.08	9.21	9.02	8.23	8.65	8.96	8.72	9.46	7.99
TA _i (± 10 $\mu\text{mol/kg}$)	M	2265	2262	2250	2250	2250	2393	2393	2393	2531	2531	2531	2531	2250
TA _{peak} (± 10 $\mu\text{mol/kg}$)	M	-	2449	2582	2611	2793	3801	4072	4430	4748	-	-	-	4608



TA _f (± 10 μmol/kg)	M	2323	2476	2640	2645	2822	3837	4110	4420	4462	1702	1835	1537	2202
DIC _i (μmol/kg)	C	2089	2073	2091	2107	2070	2192	2192	2192	2282	2287	2287	2287	2067
DIC _f (μmol/kg)	C	2113	2246	2377	2382	2540	3372	3486	3877	3389	992	1244	671	2003
Ω _{aragonite,i}	C	2.1	2.2	1.9	1.8	2.1	2.34	2.4	2.4	2.9	2.8	2.8	2.8	2.1
Ω _{aragonite-peak}	C	-	4.2	5.5	5.5	8.1	19.5	23.1	27.0	29.8	30.2	30.9	32.4	38.9
Ω _{aragonite,f}	C	2.4	2.7	3.1	3.1	3.4	5.9	7.9	7.1	13.7	6.5	5.7	7.0	2.2
CAR _f	C	-	0.92 ± 0.10	0.87 ± 0.06	0.76 ± 0.05	0.87 ± 0.04	0.84 ± 0.02	0.86 ± 0.02	0.84 ± 0.02	0.50	-	-	-	-
CAR _{equilibrium}	E	-	0.69	0.67	0.64	0.77	0.80	0.80	0.80	0.81	-	-	-	-
% equilibration (time elapsed in days)	E	(40)	130 (16)	126 (18)	116 (40)	111 (16)	104 (18)	106 (18)	104 (18)	62 (1)	(1)	(1)	(1)	(16)
CaCO ₃ precipitation?	M	-	No	No	No	No	No	No	No	No	Yes	Yes	Yes	Yes

442 The aquaria experiments are not directly comparable to the control stated in Table 2. This is because seawater for
 443 these experiments was collected in three batches between March and May 2023, with 4-6 aquaria experiments
 444 running in parallel within each set of experiments. One control aquarium was monitored for pH_T and TA changes
 445 beginning in March 2023 and concluding in May 2023. The CAR for each aquaria experiment was calculated from
 446 changes in DIC and TA between the initial ‘baseline’ and after the NaOH was added within a given aquarium, rather
 447 than between the experiment and control cases. The CAR ranged between 0.76 ± 0.05 and 0.92 ± 0.10, excluding
 448 cases where mineral precipitation was evident and for the pH_T 9.9 case where the experiment ended after one day
 449 due to a sensor logging failure. This wide range in ΔDIC/ ΔTA is likely due to the low temporal resolution of pH_T
 450 and TA samples, and the imprecision of electrode-based pH_T measurements relative to the SAMI-pH and spec-pH
 451 based measurements used in the large tank experiments.

452 With the exception of a single target pH_T 8.5 experiment, all aquaria were bubbled with ambient air, allowing for
 453 rapid CO₂ exchange, and an optically clear lid was placed on each aquarium to reduce evaporation and splashing
 454 onto nearby equipment. Some evaporation was evident from the rising TA throughout these experiments, but was
 455 not resolvable within the resolution of a handheld salinometer used for these experiments, which ranged from values
 456 of 30 - 31 during the experiments. Therefore, DIC and TA were not normalized to salinity in these cases.
 457 Temperature was discretely recorded from a combination Ross pH electrode, and temperature values ranged from 19
 458 - 21 °C during the experiments.

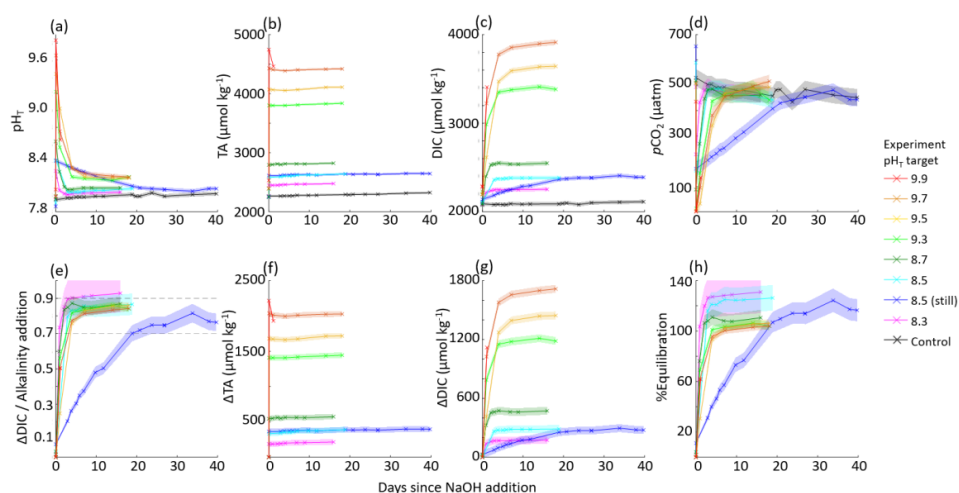
459 After the addition of NaOH, the aquaria were allowed to equilibrate with atmospheric CO₂. Similar to the large tank
 460 experiments, we used Henry’s law and CO2SYS calculations to estimate the initial and final equilibration condition
 461 of each aquaria experiment. The same average pCO_{2,atm} of 421 ± 14 ppm was used with the initial seawater
 462 temperature and salinity to estimate pCO_{2,seawater} at the beginning of each experiment. The initial equilibrium DIC
 463 was estimated from a CO2SYS calculation using this pCO_{2,seawater} and TA_i, which in all cases was less than the initial
 464 DIC calculated from TA_i and pH_{T,i} (by 36 – 36 μmol kg⁻¹). This indicates that the seawater was not fully equilibrated
 465 with the atmosphere at the time when NaOH was added, likely due to respiration and decomposition of biology
 466 removed during the bleaching step (Section 2.1), and as such, the aquaria should outgas CO₂. The final equilibrium
 467 DIC was estimated from a CO2SYS calculation using the same pCO_{2,seawater} and the TA measured just after the
 468 NaOH addition. The percent equilibration for each experiment was then estimated between the measured and
 469 predicted values for ΔDIC/ ΔTA. Due to the air bubbling, most experiments approached equilibrium with the
 470 atmosphere within 1-7 days, with the exception of the non-bubbled pH_T 8.5 experiment that took ~20 days. The
 471 surface water of this non-bubbled experiment was stagnant, and the water was only mixed via stirring just before
 472 taking pH and TA samples. Absorption of atmospheric CO₂ began immediately after the NaOH addition, as
 473 determined by decreasing pH_T. We note that there are significant uncertainties in these equilibrium estimates, and



474 that more continuous seawater carbonate chemistry measurements and finer control of bubbling and diffusion rates
475 are necessary to define the timeline for equilibration within the aquaria.

476 Each aquaria was gently stirred during the addition of NaOH to prevent $Mg(OH)_2$ precipitation. No $CaCO_3$
477 precipitation was observed in the tanks below a bulk seawater pH_T of 10.0, and TA remained stable in each of these
478 experiments with the exception of some increase driven by minor evaporation on the order of +2 $\mu\text{mol/kg}$ per day.
479 Experiments where $CaCO_3$ precipitation was induced by increasing the starting pH to values above 10 are discussed
480 in Section 3.3.

481 The aquaria experiments with target pH_T from 8.3 – 9.9 are summarized in Figure 5.



482

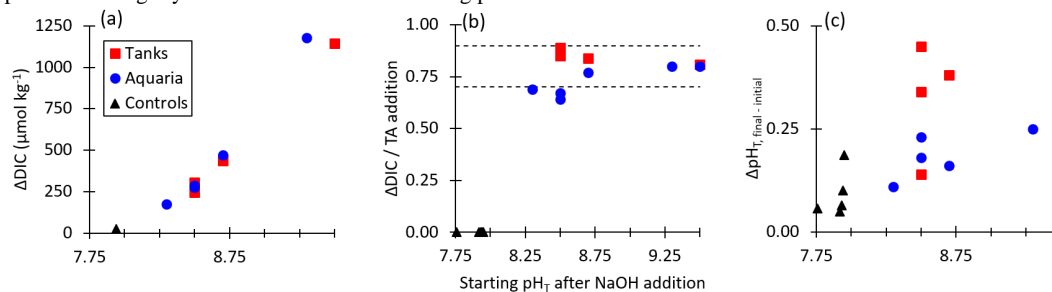
483 **Figure 5:** Results of 9 aquaria experiments in which enough NaOH was added to each aquaria to raise the bulk pH_T
484 to 8.3 – 9.9. pH_T decreased rapidly in all cases in which air bubbling sped equilibration with atmospheric CO_2 .
485 Results include: (a) measured pH_T , (b) measured TA, (c) CO2SYS-calculated DIC, (d) CO2SYS-calculated pCO_2 ,
486 (e) the observed carbon uptake ratio (CAR) as $(DIC_{\text{exp}} - DIC_{\text{baseline}}) / \Delta TA_{\text{NaOH addition}}$ with horizontal dashed lines
487 representing the expected range of 0.7-0.9 mol CO_2 uptake / mol NaOH added to seawater, the change in (f) TA and
488 (g) DIC compared to the baseline measurements before the addition of NaOH, and the percent equilibration
489 estimated between the observed and theoretical CAR.

490 In general, the large tanks and aquaria showed reasonable agreement in achieving values for CAR within the
491 expected range of 0.7-0.9 (He and Tyka, 2023). While the use of aquaria bubbled with air to speed equilibration
492 allowed for a greater range of data collection within a constrained experiment timeline, the quality of this data is
493 limited by the lack of appropriate sensors to fit into these small 15 L aquaria and fewer bottle samples due to the
494 reduced quantity of seawater. However, while the large tanks allow for a larger range of oceanographic sampling
495 and sensing techniques, it is more challenging to fully quantify mixing and circulation rates in the current large tank
496 experimental setup.

497 Figure 6 shows the dependence of the equilibrium values of ΔDIC , CAR, and $\Delta pH_T = (pH_{\text{final}} - pH_{\text{initial}})$ as a function
498 of the target starting pH_T value after alkalinity addition for both tank and aquaria experiments. Higher starting pH
499 values correspond to a greater alkalinity addition, resulting in larger values of ΔDIC relative to lower starting pH
500 values. The CAR is observed for all experiments to fall within the range typical for seawater with the temperature
501 and salinity values used in these tests. As expected from calculations of the response of the seawater carbonate



502 buffer system to additions of alkalinity, the pH_T at equilibrium exceeds the initial pH_T value prior to the addition of
503 alkalinity. That is, even once equilibrium in the alkalinity enhanced experiment tank has been reached, the ending
504 pH value is slightly elevated relative to the starting pH value.



505
506 **Figure 6:** (a) The change in final CO₂SYS-predicted DIC relative to the initial conditions for tank, aquaria, and
507 control experiments increases with increasing NaOH additions. (b) CO₂SYS-predicted CAR ($\Delta DIC / \text{Alkalinity}$
508 addition) at air-sea equilibrium conditions for tank, aquaria, and control experiments, with horizontal dashed lines
509 representing the expected range of 0.7-0.9 mol CO₂ uptake / mol NaOH added to seawater. (c) The CO₂SYS-
510 predicted $\Delta pH_T = (pH_{\text{final}} - pH_{\text{initial}})$ increases as a function of the target pH_T value after alkalinity addition for both
511 tank and aquaria experiments.

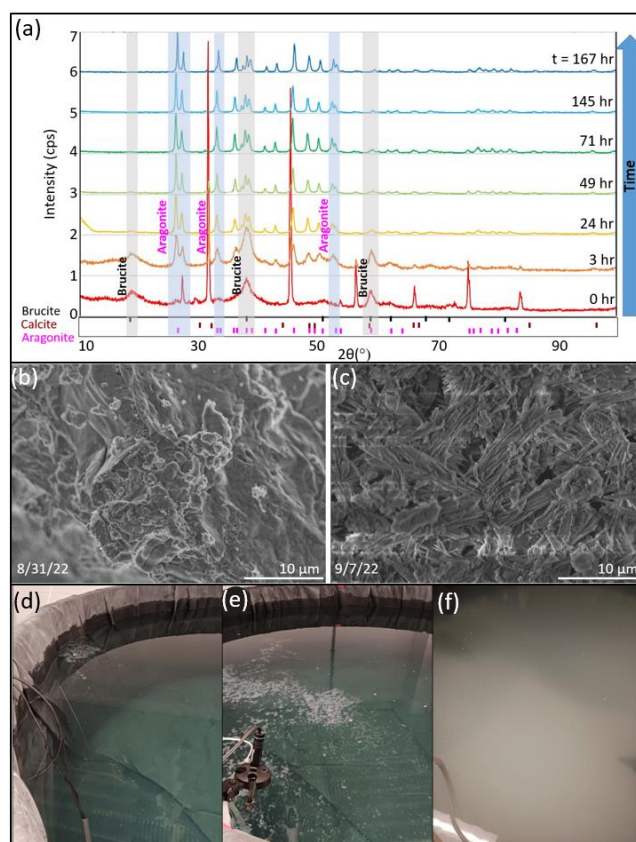
512 3.3 Experiments exceeding the CaCO₃ precipitation threshold

513 While Mg(OH)₂ precipitation occurs immediately upon introduction of NaOH to still seawater, it may be rapidly
514 dissolved or avoided entirely by gentle mixing, including via the use of stirrers, circulation pumps, or air bubblers.
515 This precipitation and redissolution happened rapidly enough that it was not identified in any TA or other variables
516 measured in the aquaria and tank tests. However, in cases where enough NaOH was added to raise the bulk seawater
517 pH_T to greater than 10.0 (i.e. in one large tank test with a target pH_T of 10.3, and in 4 aquaria experiments ranging
518 from pH_T 10.0-10.3), runaway precipitation of Mg(OH)₂ and CaCO₃ was observed. This was characterized by a
519 sharp reduction in both TA and DIC and an increase in turbidity.

520 In both the tank and aquarium pH_T 10.3 cases, discrete samples of the precipitate were collected at seven different
521 times after the bulk pH_T value reached 10.3 (0h, 3h, 24h, 49h, 71h, 145h, 167h - see Fig. 6) for XRD and SEM
522 analysis. At each timepoint, 0.5 – 1 L seawater was collected from the tank sampling port or from the center of the
523 aquaria. In cases where precipitation had visibly settled at the bottom of the aquaria, this material was stirred into the
524 water column before sampling. We note that material that settled to the bottom of the large tanks was not directly
525 collected, and that only a subset of precipitation was collected at each time point, such that later timepoints may
526 include solids that had precipitated at the beginning of the experiment. The filtered seawater was immediately
527 analyzed for TA and pH via Ross electrode because the heightened pH was out of the range of spectrophotometric
528 methods. Bottle samples of filtered seawater were not able to be analyzed at NOAA PMEL due to the continued
529 precipitation of CaCO₃ after filtration and preservation. Both XRD and SEM results showed the dominance of
530 Mg(OH)₂ precipitation immediately after the alkalinity addition and the corresponding increase in pH and $\Omega_{\text{aragonite}}$
531 (to a value of around 30), though this signal was partially obscured by the presence of other salts. The Mg(OH)₂
532 precipitation at this stage was thick, slurry-like, and difficult to appropriately rinse. Within hours of the NaOH
533 addition, the runaway CaCO₃ precipitation began, characterized by fine, light particulates in the water column and a
534 sharp increase in turbidity. Within ~24 hours of the NaOH addition, most Mg(OH)₂ signals had disappeared, leaving
535 only aragonite and calcite peaks in the XRD. The results of the XRD analysis for the tank experiment are
536 summarized in Figure 7, and the aquarium experiment showed similar results. TA decreased throughout the
537 precipitation of Mg(OH)₂ and CaCO₃, and was below that of the initial seawater within 24 hours of the NaOH
538 addition. In the tank experiment, the initial TA (2025 $\mu\text{mol/kg}$) was raised by 3305 $\mu\text{mol/kg}$. Within 3 days the TA



539 had decreased to 1583 $\mu\text{mol/kg}$ and continued to decrease through the termination of the experiment to 1253
540 $\mu\text{mol/kg}$ 10 days after the addition of NaOH. The DIC, which was initially measured at 1938 $\mu\text{mol/kg}$, decreased to
541 720 $\mu\text{mol/kg}$ by the end of the experiment. This experiment shows that runaway CaCO_3 can result in a significant
542 loss of both efficiency of alkalinity dosing for OAE projects and of storage of carbon in the form of DIC. A figure of
543 time-series data collected during the tank experiment is available in the supplementary materials.



544

545 **Figure 7:** (a) XRD analysis (top) of particulates filtered from seawater after the addition of enough NaOH to raise
546 the bulk seawater pH_T to 10.3 showed mineral precipitation initially dominated by $\text{Mg}(\text{OH})_2$ before it was overtaken
547 by $\text{CaCO}_{3,\text{arag}}$. The shaded grey vertical bars highlight peaks characteristic of brucite which typically disappear after
548 24 hours, and the shaded blue bars represent several aragonite peaks which appear between 3 and 24 hours.
549 Representative SEM images show (b) $\text{Mg}(\text{OH})_2$ captured ~3 hours after the NaOH addition, and (c) $\text{CaCO}_{3,\text{arag}}$ at the
550 end of the experiment. Photographs of the tank experiment show seawater (d) before NaOH addition, (e) during
551 NaOH addition into still water (i.e., without the use of stirrers, circulation pumps, or air bubblers to break up and
552 redissolve $\text{Mg}(\text{OH})_2$), and (f) ~3 hours after the NaOH addition, when runaway CaCO_3 precipitation became visually
553 apparent.

554 In summary, the presence and duration of brucite precipitation upon addition of 0.5 M aqueous NaOH depends on
555 the ratio of the NaOH addition rate to the local dilution rate in the receiving waters. Future research using flow
556 through tanks could help identify thresholds below which brucite precipitation can be avoided or limited. At the
557 given initial seawater conditions, the threshold for aragonite precipitation begins at an Ω_{arag} of 30, corresponding to



558 $\text{pH}_T > 10.0$. The potential for this precipitation may be reduced by active mixing at the point of NaOH introduction,
559 maintaining a mixing volume below bulk seawater pH_T of 10.0, and allowing for appropriate dilution in flow-
560 through conditions.

561 **5 Summary**

562 These results demonstrate that ocean alkalinity enhancement using aqueous sodium hydroxide in seawater results in
563 CO_2 removal from air at an efficiency of $0.75 (\pm 0.04) - 0.92 (\pm 0.10)$, with 90% equilibration typically achieved
564 within 7 - 9 weeks (still surface water with ~ 16 L/min subsurface circulation through UV arrays) to 3 - 5 weeks
565 (with the addition of ambient air bubbling into the bottom of each tank) of the initial addition when performed in
566 ~ 6000 L tanks with seawater-air contact areas of around 4.6 m^2 . Here, uncertainties are driven by sensor precision
567 and temporal resolution in discrete DIC and TA sampling, the limited number of experiments with minimal
568 opportunities for duplicates or replicates, and poorly constrained data on mixing, circulation, and air bubbling rates.
569 Ongoing experiments seek to improve each of these conditions and should particularly focus on constraining the
570 movement of water within a given tank to improve air-sea equilibration estimates and to allow for better
571 extrapolation from tank to field experiments. In addition, a focus of ongoing and future work is to provide rate
572 estimates for the uptake of atmospheric CO_2 in response to an NaOH addition, allowing for fitting and extrapolation
573 of a shortened experiment to equilibration with the atmosphere.

574 We relied on several methods to constrain seawater carbonate chemistry. The tank-scale experiments primarily
575 relied on discrete (\leq daily) DIC and TA sampling (NOAA PMEL), paired with daily measurements from
576 spectrophotometric pH systems (SAMI-pH and a semi-automated benchtop spec-pH system following Carter et al.
577 (2013)) and local TA measurements. With appropriate calibration or correction of the spec-pH systems relative to
578 CRM, there was no significant difference in carbonate calculations using the NOAA PMEL DIC-TA or spec-pH-
579 local TA pairings, though the latter case typically produced larger uncertainties. Aquaria experiments relied on a
580 standard glass pH electrode ($<$ daily, corrected to spectrophotometric systems) with discrete ($<$ daily) TA
581 measurements, which provided reasonable data relative to the tank experiments. As a result, ongoing tank-scale
582 experiments have limited the volume of discrete DIC and TA samples collected for analysis at NOAA PMEL to
583 allow for faster and less expensive monitoring via spec-pH and local TA titrations. However, we note that the major
584 limitation in this measurement pathway lies in the spec-pH method, which is typically limited to pH_T measurements
585 ranging from 7 - 9 for the meta-cresol purple indicator dye used. While our measurements retained some sensitivity
586 up to $\text{pH}_T 9.5$, such a method should typically be considered unreliable at these pH_T values, and we relied on
587 frequent correction to CRM and comparison with DIC/TA samples. Thymol blue is an alternative
588 spectrophotometric pH_T indicator dye with sensitivity over the higher pH_T conditions observed during these initial
589 trials and will be assessed for future experiments.

590 Aqueous NaOH with concentrations as high as 0.5 M can be added directly to turbulent seawater with only limited
591 observable precipitation of $\text{Mg}(\text{OH})_2$. In these conditions this precipitated mineral rapidly redissolves on the
592 timescales of minutes to seconds. Improved control over the NaOH dosing rate (in our tank experiments, ~ 50 mL
593 NaOH/min) and the turbulence of the receiving water through metered flow through experiments will be valuable in
594 extrapolating to field conditions. This precipitation is detectable both visually and through turbidity measurements
595 and implies that straightforward measurement of pH and turbidity at the dispersal site can be used to adjust the
596 alkalinity dispersal rate according to local mixing conditions such that $\text{Mg}(\text{OH})_2$ precipitation is avoided and/or
597 redissolves when it occurs. No significant CaCO_3 precipitation was observed at $\text{pH} < 10.0$ or $\Omega_{\text{aragonite}} < 30.0$.
598 Runaway CaCO_3 precipitation was observed above these thresholds, where a massive precipitation and settling of
599 $\text{Mg}(\text{OH})_2$ and CaCO_3 solids results in less alkalinity in the overlying water than at the starting condition. pH and
600 turbidity sensing combined with discrete TA measurements could be used as a feedback signal for alkalinity dosing
601 into seawater to ensure that the local maximum thresholds at the dispersal location do not approach or exceed
602 conditions that promote significant CaCO_3 precipitation. We note that future investigations seeking to better



603 approximate field conditions should take into account seasonal and tidal shifts in temperature and salinity, and
604 varying conditions of suspended sediment in the water column, including that of aerial dust, terrestrial runoff, and
605 resuspended bottom sediments.

606 In these experiments, the seawater was filtered and bleach treated prior to experiments to limit biological growth,
607 and both tank and aquaria experiments were conducted indoors with limited light. Nevertheless, in most
608 experiments, biological growth was observed after a few weeks, including cyanobacteria and coccolithophores. A
609 series of experiments are underway to test the difference in CO₂ removal efficiency for two side-by-side tanks, both
610 of which are dosed with NaOH, but only one of which was bleached. Preliminary results show minimal difference
611 between the bleached and unbleached tanks, indicating these experiments are applicable to real-world conditions, at
612 least for regions with biological communities similar to that of Long Island Sound, but further investigation is
613 warranted.

614 A focus of future work is to consider the potential impact of the SEAMATE process on local ocean acidification
615 mitigation efforts. We note that in each constrained tank and aquaria experiment, the pH_T at equilibrium exceeds the
616 initial pH_T value prior to the addition of alkalinity. A controlled release of alkalinity could theoretically be
617 configured to maintain a locally elevated pH_T value relative to pre-alkaline conditions, with potential uses in
618 aquaculture and hatchery environments.

619 These results provide clear and practical guidelines for MRV for OAE implementations employing aqueous
620 alkalinity. First, carbonate chemistry and turbidity measurements at the alkalinity dispersal location can ensure that
621 seawater parameters such as pH and $\Omega_{\text{aragonite}}$ remain within pre-determined safe bounds and that unwanted
622 precipitation is avoided. Second, for a given OAE deployment, where ocean models provide a reasonable certainty
623 about the fraction of the alkalinity plume remaining in the surface over weeks to months, the CO₂ removal efficiency
624 and timescale for air-seawater equilibration provided by our experiments can place a lower bound on the amount of
625 CO₂ removal expected from that OAE intervention. Expanding these studies from tank scale to mesocosm and field
626 experiments will be crucial to understanding biological impacts and constraining realistic air-sea interactions in
627 response to this type of OAE.

628 **Data availability**

629 Data are described in the manuscript and provided Supplementary Materials, which includes a .csv file with
630 processed sensor and sample time-series data at hourly resolution.

631 **Author contribution**

632 MDE and BRC designed the experiments and MCR carried them out with support from NH, CS, and XL. JH
633 provided support on experimental setup and instrumentation. MCR prepared the manuscript with contributions from
634 all co-authors.

635 **Competing interests**

636 MCR is Lead Oceanographer and Head of MRV at Ebb Carbon, Inc. MDE is Co-Founder and Chief Scientific
637 Advisor at Ebb Carbon, Inc.

638 **Acknowledgements**

639 We would like to thank Stephen Abrams and Thomas Wilson at Stony Brook University Flax Pond Marine Lab for
640 technical assistance in experiment setup. We thank Chris Ikeda and Susan Curless of NOAA PMEL for support in



641 discrete sample analysis. We thank Mike Tyka for productive discussions. We thank Eyal Wurgaft for assistance in
642 TA titrations.

643 **Funding**

644 We acknowledge funding from The Grantham Foundation for the Protection of the Environment under the SEA
645 MATE (Safe Elevation of Alkalinity for the Mitigation of Acidification Through Electrochemistry) grant. In
646 addition, this research used the XRD facility of the Center for Functional Nanomaterials (CFN), which is a U.S.
647 Department of Energy Office of Science User Facility, at Brookhaven National Laboratory under Contract No. DE-
648 SC0012704. BRC and JH were funded through the Cooperative Institute for Climate, Ocean, and Ecosystem
649 Studies (CICOES) under NOAA Cooperative Agreement NA20OAR4320271 and supported by NOAA's PMEL.

650 **References**

- 651
652 Albright, R., Caldeira, L., Hoffelt, J., Kwiatkowski, L., Maclaren, J.K., Mason, B.M., Nebuchina, Y. et al.: Reversal
653 of ocean acidification enhances net coral reef calcification. *Nature*, 531, no. 7594: 362-365, 2016.
654 Bach, L. T., Gill, S.J., Rickaby, R.E.M., Gore, S., and Renforth, P.: CO₂ removal with enhanced weathering and
655 ocean alkalinity enhancement: potential risks and co-benefits for marine pelagic ecosystems. *Frontiers in*
656 *Climate*, 1, 7, 2019.
657 Berner, R. A., Lasaga, A.C., and Garrels, R.M.: Carbonate-silicate geochemical cycle and its effect on atmospheric
658 carbon dioxide over the past 100 million years. *Am. J. Sci.:(United States)* 283, no. 7, 1983.
659 Boettcher, M., Chai, F. Cullen, J., Goeschl, T., Lampitt, R., Lenton, A., Oeschles, A. et al.: High level review of a
660 wide range of proposed marine geoengineering techniques. *GESAMP Working Group Reports and Studies*, 41,
661 2019.
662 Carter, B. R., J. A. Radich, H. L. Doyle, and A. G. Dickson.: An automated system for spectrophotometric seawater
663 pH measurements. *Limnology and Oceanography: Methods*, 11, no. 1: 16-27, 2013.
664 Caserini, S., Storni, N., & Grosso, M.: The availability of limestone and other raw materials for ocean alkalinity
665 enhancement. *Global Biogeochemical Cycles*, 36, e2021GB007246. <https://doi.org/10.1029/2021GB007246>,
666 2022.
667 Cyronak, T., Albright, R., and Bach, L.: Chapter 4.5: Field Experiments, *State Planet Discuss.* [preprint],
668 <https://doi.org/10.5194/sp-2023-9>, in review, 2023.
669 de Lannoy, C.-F., Eisaman, M.D., Jose, A., Karnitz, S.D., DeVaul, R.W., Hannun, K., and Rivest, J.L.B.: Indirect
670 ocean capture of atmospheric CO₂: Part I. Prototype of a negative emissions technology. *International journal of*
671 *greenhouse gas control*, 70: 243-253, 2018.
672 Dickson, A. G.: An exact definition of total alkalinity and a procedure for the estimation of alkalinity and total
673 inorganic carbon from titration data. *Deep Sea Research Part A. Oceanographic Research Papers*, 28(6), 609–
674 623, 1981.
675 Dickson, A. G.: The development of the alkalinity concept in marine chemistry. *Marine Chemistry*, 40(1–2), 49–63,
676 1992.
677 Dickson, A.G.: Thermodynamics of the dissociation of boric acid in synthetic seawater from 273.15 to 318.15 K.
678 *Deep Sea Research Part A. Oceanographic Research Papers*, 37, no. 5: 755-766, 1990.
679 Dickson, A.G., Sabine, C.L., and Christian, J.R.: Guide to best practices for ocean CO₂ measurements. *North Pacific*
680 *Marine Science Organization*, 2007.
681 Eisaman, M. D., Parajuly, K., Tuganov, A., Eldershaw, C., Chang, N., Littau, K. A. CO₂ Extraction from Seawater
682 Using Bipolar Membrane Electrodialysis, *Energy Environ. Sci.*, 5: 7346. <https://doi.org/10.1039/c2ee03393c>,
683 2012.
684 Eisaman, M. D.; Rivest, J. L. B.; Karnitz, S. D.; De Lannoy, C.-F.; Jose, A.; DeVaul, R. W.; Hannun, K. Indirect
685 Ocean Capture of Atmospheric CO₂: Part II. Understanding the Cost of Negative Emissions. *International*
686 *Journal of Greenhouse Gas Control*, 70: 254–261, <https://doi.org/10.1016/j.ijggc.2018.02.020>, 2018.
687 Eisaman, M. D., Geilert, S., Renforth, P., Bastianini, L., Campbell, J., Dale, A. W., Foteinis, S., Grasse, P., Hawrot,
688 O., Löscher, C. R., Rau, G. H., and Rønning, J.: Assessing the technical aspects of ocean-alkalinity-
689 enhancement approaches, in: *Guide to Best Practices in Ocean Alkalinity Enhancement Research*, edited by:
690 Oeschles, A., Stevenson, A., Bach, L. T., Fennel, K., Rickaby, R. E. M., Satterfield, T., Webb, R., and Gattuso,
691 J.-P., Copernicus Publications, State Planet, 2-oae2023, 3, <https://doi.org/10.5194/sp-2-oae2023-3-2023>, 2023.



- 692 Feely, R.A., Alin, S., Carter, B., Bednaršek, N., Hales, B., Chan, F., Hill, T.M., Gaylord, B., Sanford, E., Byrne,
693 R.H., Sabine, C.L., Greeley, D., Juraneck, L., Chemical and biological impacts of ocean acidification along the
694 west coast of North America, *Estuarine, Coastal and Shelf Science*, doi: 10.1016/j.ecss.2016.08.043, 2016.
- 695 Feng, E. Y., Koeve, W., Keller, D.P., and Oschlies, A.: Model-Based Assessment of the CO₂ Sequestration Potential
696 of Coastal Ocean Alkalinization. *Earth's Future*, 5, no. 12: 1252-1266, 2017.
- 697 Fennel, K., Long, M. C., Algar, C., Carter, B., Keller, D., Laurent, A., Mattern, J. P., Musgrave, R., Oschlies, A.,
698 Ostiguy, J., Palter, J., and Whitt, D. B.: Modeling considerations for research on Ocean Alkalinity Enhancement
699 (OAE), *State Planet Discuss.* [preprint], <https://doi.org/10.5194/sp-2023-10>, in review, 2023.
- 700 Ferderer, A., Chase, Z., Kennedy, F., Schulz, K.G., and Bach, L.T.: Assessing the influence of ocean alkalinity
701 enhancement on a coastal phytoplankton community. *Biogeosciences* 19, no. 23: 5375-5399, 2022.
- 702 Friis, K.; Körtzinger, A.; Wallace, D. W. R. The Salinity Normalization of Marine Inorganic Carbon Chemistry
703 Data. *Geophys. Res. Lett.*, 30 (2). <https://doi.org/10.1029/2002GL015898>, 2003.
- 704 Hartmann, J., Suitner, N., Lim, C., Schneider, J., Marín-Samper, L., Arístegui, J., Renforth, P., Taucher, J., and
705 Riebesell, U.: Stability of alkalinity in ocean alkalinity enhancement (OAE) approaches—consequences for
706 durability of CO₂ storage. *Biogeosciences* 20, no. 4: 781-802, 2023.
- 707 Harvey, L.: Mitigating the atmospheric CO₂ increase and ocean acidification by adding limestone powder to
708 upwelling regions, *Journal of 640 Geophysical Research: Oceans*, 113, 2008.
- 709 He, J. and Tyka, M. D.: Limits and CO₂ equilibration of near-coast alkalinity enhancement, *Biogeosciences*, 20, 27–
710 43, <https://doi.org/10.5194/bg-20-27-2023>, 2023.
- 711 Ho, D. T., Bopp, L., Palter, J. B., Long, M. C., Boyd, P., Neukermans, G., and Bach, L.: Chapter 6: Monitoring,
712 Reporting, and Verification for Ocean Alkalinity Enhancement, *State Planet Discuss.* [preprint],
713 <https://doi.org/10.5194/sp-2023-2>, in review, 2023.
- 714 Ilyina, T., Wolf-Gladrow, D., Munhoven, G., and Heinze, C.: Assessing the potential of calcium-based artificial
715 ocean alkalinization to mitigate rising atmospheric CO₂ and ocean acidification, *Geophysical Research Letters*,
716 40, 5909-5914, 2013.
- 717 IPCC: Summary for Policymakers. In: *Climate Change 2021: The Physical Science Basis, Contribution of Working*
718 *Group I to the Sixth Assessment Report of the Intergovernmental Panel on Climate Change*, edited by: Masson-
719 Delmotte, V., Zhai, P., Pirani, A., Connors, S. L., Péan, C., Berger, S., Caud, N., Chen, Y., Goldfarb, L., Gomis,
720 M. I., Huang, M., Leitzell, K., Lonnoy, E., Matthews, J. B. R., Maycock, T. K., Waterfield, T., Yelekçi, O., Yu,
721 R., and Zhou, B.: Cambridge University Press, Cambridge, United Kingdom and New York, NY, USA, 3–32,
722 <https://doi.org/10.1017/9781009157896.001>, 2022.
- 723 Isson, T. T., Planavsky, N. J., Coogan, L. A., Stewart, E. M., Ague, J. J., Bolton, E. W., et al.: Evolution of the
724 global carbon cycle and climate regulation on earth. *Global Biogeochemical Cycles*, 34, e2018GB006061.
725 <https://doi.org/10.1029/2018GB006061>, 2020.
- 726 Jones, D.C., Ito, T., Takano, Y., and C.-W Hsu, C.-W.: Spatial and seasonal variability of the air-sea equilibration
727 timescale of carbon dioxide. *Global Biogeochemical Cycles*, 28(11), 1163–1178,
728 <https://doi.org/10.1002/2014GB004813>, 2014.
- 729 Kheshgi, H. S.: Sequestering atmospheric carbon dioxide by increasing ocean alkalinity, *Energy*, 20, 915-922, 1995.
- 730 Köhler, P., Hartmann, J., and Wolf-Gladrow, D.A.: Geoengineering potential of artificially enhanced silicate
731 weathering of olivine. *Proceedings of the National Academy of Sciences* 107, no. 47: 20228-20233, 2010.
- 732 La Plante, E., Chen, X., Bustillos, S., Bouissonnie, A., Traynor, T., Jassby, D., Corsini, L., Simonetti, D., and Sant,
733 G.: Electrolytic seawater mineralization and the mass balances that demonstrate carbon dioxide removal. *ACS*
734 *EST Engg.* <https://doi.org/10.1021/acsestengg.3c00004>, 2023.
- 735 Lee, K., Kim, T.-W., Byrne, R.H., Millero, F.J., Feely, R.A., and Liu, Y.-M.: The universal ratio of boron to
736 chlorinity for the North Pacific and North Atlantic oceans. *Geochimica et Cosmochimica Acta* 74, no. 6: 1801-
737 1811, 2010.
- 738 Lewis, E., Wallace, D., & Allison, L. J.: Program developed for CO₂ system calculations.
739 <https://doi.org/10.2172/639712>, 1998.
- 740 Lu, X., Ringham, M., Hirtle, N., Hillis, K., Shaw, C., Herndon, J., Carter, B.R., and Eisaman, M.D.:
741 Characterization of an Electrochemical Approach to Ocean Alkalinity Enhancement. In *AGU Fall Meeting*
742 *Abstracts*, vol. 2022, pp. GC31C-01. 2022.
- 743 Lueker, T.J., Dickson, A.G., and Keeling, C.D.: Ocean pCO₂ calculated from dissolved inorganic carbon, alkalinity,
744 and equations for K₁ and K₂: validation based on laboratory measurements of CO₂ in gas and seawater at
745 equilibrium. *Marine chemistry* 70, no. 1-3: 105-119, 2000.
- 746 Minx, J.C., Lamb, W.F., Callaghan, M.W., Fuss, S., Hilaire, J., Creutzig, F., Amann, T., et al.: Negative
747 emissions—Part 1: Research landscape and synthesis. *Environmental Research Letters* 13, no. 6: 063001, 2018.



- 748 Montserrat, F., Renforth, P., Hartmann, J., Leermakers, M., Knops, P., and Meysman, F.J.R.: Olivine dissolution in
749 seawater: implications for CO₂ sequestration through enhanced weathering in coastal environments.
750 *Environmental Science & Technology* 51, no. 7: 3960-3972, 2017.
- 751 Moras, C.A., Bach, L.T., Cyronak, T., Joannes-Boyau, R., and Schulz, K.G.: Ocean alkalinity enhancement–
752 avoiding runaway CaCO₃ precipitation during quick and hydrated lime dissolution. *Biogeosciences* 19, no. 15:
753 3537-3557, 2022.
- 754 National Academies of Sciences, Engineering, and Medicine. A research strategy for ocean-based carbon dioxide
755 removal and sequestration. 2021.
- 756 National Academies of Sciences, Engineering, and Medicine. Negative Emissions Technologies and Reliable
757 Sequestration: A Research Agenda. 2018.
- 758 Nduagu, E."Production of Mg(OH)₂ from Mg-silicate rock for CO₂ mineral sequestration. Dissertation for Abo
759 Akademi University, 2012.
- 760 Oeschies, A., Bach, L., Rickaby, R., Satterfield, T., Webb, R. M., and Gattuso, J.-P.: Climate targets, carbon dioxide
761 removal and the potential role of Ocean Alkalinity Enhancement, *State Planet Discuss.* [preprint],
762 <https://doi.org/10.5194/sp-2023-13>, in review, 2023.
- 763 Pierrot, D., Lewis, E., and Wallace, D.W.R.: MS Excel program developed for CO₂ system calculations.
764 ORNL/CDIAC-105a. Carbon Dioxide Information Analysis Center, Oak Ridge National Laboratory, U.S.
765 Department of Energy, Oak Ridge, Tennessee, 2006.
- 766 Rau, G.H.: Electrochemical splitting of calcium carbonate to increase solution alkalinity: Implications for mitigation
767 of carbon dioxide and ocean acidity. *Environmental science & technology* 42, no. 23: 8935-8940, 2008.
- 768 Renforth, P., and Henderson, G.: Assessing ocean alkalinity for carbon sequestration. *Reviews of Geophysics* 55,
769 no. 3: 636-674, 2017.
- 770 Rigopoulos, I., Harrison, A.L., Delimitis, A., Ioannou, I., Efstathiou, A.M., Kyratsi, T., and Oelkers, E.H. : Carbon
771 sequestration via enhanced weathering of peridotites and basalts in seawater. *Applied Geochemistry* 91: 197-
772 207, 2018.
- 773 Rueda, O., Mogollón, J.M., Tukker, A., and Scherer, L.: Negative-emissions technology portfolios to meet the 1.5°
774 C target. *Global Environmental Change* 67: 102238, 2021.
- 775 Rogelj, J., Popp, A., Calvin, K. V., Luderer, G., Emmerling, J., Gernaat, D., Fujimori, S., Strefler, J., Hasegawa, T.,
776 Marangoni, G., Krey, V., Kriegler, E., Riahi, K., van Vuuren, D. P., Doelman, J., Drouet, L., Edmonds, J.,
777 Fricko, O., Harmsen, M., Havlík, P., Humpenöder, F., Stehfest, E., and Tavoni, M.: Scenarios towards limiting
778 global mean temperature increase below 1.5 °C, *Nat. Clim. Change*, 8, 325–332, [https://doi.org/10.1038/s41558-](https://doi.org/10.1038/s41558-018-0091-3)
779 018-0091-3, 2018.
- 780 Schulz, K. G., Bach, L. T., and Dickson, A. G.: Seawater carbonate system considerations for ocean alkalinity
781 enhancement research, *State Planet Discuss.* [preprint], <https://doi.org/10.5194/sp-2023-12>, in review, 2023.
- 782 Shaw, C., Ringham, M.C., Lu, X., Carter, B.R., Eisaman, M.D., and Tyka, M.: Understanding the Kinetics of
783 Electrochemically derived Magnesium Hydroxide for Ocean Alkalinity Enhancement. In *AGU Fall Meeting*
784 *Abstracts*, vol. 2022, pp. GC32I-0713. 2022.
- 785 Song, S., Wang, Z.A., Gonnee, M.E., Kroeger, K.D., Chu, S.N., Li, D., and Liang, H.: An important
786 biogeochemical link between organic and inorganic carbon cycling: Effects of organic alkalinity on carbonate
787 chemistry in coastal waters influenced by intertidal salt marshes. *Geochimica et Cosmochimica Acta* 275:123-
788 139, 2020.
- 789 Tyka, M.D., Arsdale, C.V., and Platt, J.C.: CO₂ capture by pumping surface acidity to the deep ocean. *Energy &*
790 *Environmental Science* 15, no. 2: 786-798, 2022.
- 791 Van Heuven, S., Pierrot, D., Rae, J., Lewis, E., & Wallace, D.: MATLAB program developed for CO₂ system
792 calculations. ORNL/CDIAC-105b, 530, 2011.
- 793 Vitillo, J. G., Eisaman, M.D., Aradóttir, E.S.P., Passarini, F., Wang, T., and Sheehan, S.W.: The role of carbon
794 capture, utilization and storage for economic pathways that limit global warming to below 1.5° C." *Iscience*:
795 104237, 2022.
- 796 Wang, Z. A. and Cai, W. J.: Carbon dioxide degassing and inorganic carbon export from a marsh-dominated estuary
797 (the Duplin River): A marsh CO₂ pump. *Limnol. Oceanogr.* 49, 341–354, 2004.
- 798 Wolf-Gladrow, D. A., Zeebe, R. E., Klaas, C., Körtzinger, A., & Dickson, A. G.: Total alkalinity: The explicit
799 conservative expression and its application to biogeochemical processes. *Marine Chemistry*, 106(1–2), 287–
800 300, 2007.
- 801 Wang, H., Pilcher, D. J., Kearney, K. A., Cross, J. N., Shugart, O. M., Eisaman, M. D., & Carter, B. R.: Simulated
802 impact of ocean alkalinity enhancement on atmospheric CO₂ removal in the Bering Sea. *Earth's Future*, 11(1),
803 e2022EF002816, 2023